X-ray structure of human aquaporin 2 and its implications for nephrogenic diabetes insipidus and trafficking

Anna Frick[a], Urszula Kosinska Eriksson[a], Fabrizio de Mattia[b], Fredrik Öberg[a], Kristina Hedfalk[a], Richard Neutze[a], Willem J. de Grip[c], Peter M. T. Deen[b], and Susanna Törnroth-Horsefield[a,d,1]

[a]Department of Chemistry and Molecular Biology, University of Gothenburg, 405 30 Gothenburg, Sweden; [b]Department of Physiology, Radboud University Medical Center, 6500 HB, Nijmegen, The Netherlands; [c]Department of Biochemistry, Radboud Institute for Molecular Life Sciences, Radboud University Medical Center, G525 GA, Nijmegen, The Netherlands; and [d]Department of Biochemistry and Structural Biology, Centre for Molecular Protein Science, Lund University, 221 00 Lund, Sweden

Edited* by Robert M. Stroud, University of California, San Francisco, CA, and approved March 20, 2014 (received for review November 15, 2013)

Human aquaporin 2 (AQP2) is a water channel found in the kidney collecting duct, where it plays a key role in concentrating urine. Water reabsorption is regulated by AQP2 trafficking between intracellular storage vesicles and the apical membrane. This process is tightly controlled by the pituitary hormone arginine vasopressin and defective trafficking results in nephrogenic diabetes insipidus (NDI). Here we present the X-ray structure of human AQP2 at 2.75 Å resolution. The C terminus of AQP2 displays multiple conformations with the C-terminal α-helix of one protomer interacting with the cytoplasmic surface of a symmetry-related AQP2 molecule, suggesting potential protein–protein interactions involved in cellular sorting of AQP2. Two Cd^{2+}-ion binding sites are observed within the AQP2 tetramer, inducing a rearrangement of loop D, which facilitates this interaction. The locations of several NDI-causing mutations can be observed in the AQP2 structure, primarily situated within transmembrane domains and the majority of which cause misfolding and ER retention. These observations provide a framework for understanding why mutations in AQP2 cause NDI as well as structural insights into AQP2 interactions that may govern its trafficking.

membrane protein | X-ray crystallography | water channel protein

Water is the major ingredient of the human body, constituting 55–65% of our total body weight (1). Water homeostasis is maintained by the kidneys, which filter ∼180 L of primary urine every day. Although most water is constitutively reabsorbed in the proximal tubules and descending limbs of Henle (2), the body's water balance is fine-tuned by regulated water reabsorption, which takes place in the kidney collecting duct. Water reabsorption is mediated by aquaporins, membrane-bound water channels, of which seven of the 13 human isoforms have been located in the human kidney (3). Of these, human aquaporin 2 (AQP2) is present in the principal cells of the collecting duct and is responsible for regulated water reabsorption.

AQP2 is stored in intracellular vesicles under water-saturating conditions. When the levels of the pituitary antidiuretic hormone arginine vasopressin (AVP) are elevated in response to dehydration or hypernatremia, AVP binding to the vasopressin 2 receptor (V2R) in the basolateral membrane stimulates an increase in intracellular cAMP. This triggers the phosphorylation of Ser256 in the AQP2 C terminus by protein kinase A (PKA) and flags the protein for trafficking from storage vesicles to the apical membrane (4–6). AVP also triggers additional phosphorylation at Ser264 and Ser269 (7, 8), with all three sites being phosphorylated in AQP2s targeted to the plasma membrane (9). The resulting redistribution of AQP2 increases transcellular water permeability and concentrates urine (Fig. S1). Once correct water balance is restored, AQP2 is internalized through ubiquitin-mediated endocytosis and redirected to storage vesicles or targeted for degradation (10–12).

Because of its central role in water homeostasis, dysregulation of AQP2 is implicated in several human disease states including congestive heart failure, liver cirrhosis, and preeclampsia (13). Failure to recruit AQP2 to the apical membrane underlies acquired and congenital nephrogenic diabetes insipidus (NDI), a water balance disorder in which patients lack the ability to concentrate urine, leading to severe dehydration (14). Although congenital NDI is most commonly caused by mutations in the gene for the V2R receptor, around 10% of NDI patients harbor AQP2 gene mutations. NDI-causing AQP2 mutations either interfere with its shuttling from storage vesicles to the apical membrane or, more frequently, cause misfolding and retention in the endoplasmic reticulum (ER) (15, 16).

Here we present the X-ray structure of human AQP2 at 2.75 Å resolution, providing a structural framework that contributes to our understanding of AQP2 trafficking as well as gives insight into the mechanism of how AQP2 mutations induce NDI. This structure reveals significant positional variability of the short AQP2 C-terminal helix. In one protomer, this region interacts with the cytoplasmic surface of a symmetry-related AQP2 molecule, an interaction that may mimic protein–protein interactions involved in AQP2 cellular sorting. Moreover, two Cd^{2+} ions (presumably Ca^{2+} in vivo) are observed to bind the AQP2

Significance

Human aquaporin 2 (AQP2) is found in the kidney collecting duct, where it translocates water across the apical membrane and is crucial for urine concentration. AQP2 is regulated by trafficking between intracellular storage vesicles and the apical membrane, a process that is tightly controlled by the pituitary hormone arginine vasopressin. Defective AQP2 trafficking leads to nephrogenic diabetes insipidus (NDI), a water balance disorder characterized by large urine volumes, leading to dehydration. We have solved the X-ray structure of human AQP2 at 2.75 Å resolution. This structure deepens our molecular understanding of AQP2 trafficking, as well as serves as a structural scaffold for understanding why AQP2 mutations cause NDI.

Author contributions: A.F., F.Ö., K.H., R.N., W.J.d.G., P.M.T.D., and S.T.-H. designed research; A.F., U.K.E., F.d.M., F.Ö., and S.T.-H. performed research; A.F., R.N., P.M.T.D., and S.T.-H. analyzed data; and A.F., R.N., W.J.d.G., P.M.T.D., and S.T.-H. wrote the paper.

The authors declare no conflict of interest.

*This Direct Submission article had a prearranged editor.

Data deposition: The atomic coordinates have been deposited in the Protein Data Bank, www.pdb.org (PDB ID code 4NEF).

[1]To whom correspondence should be addressed. E-mail: susanna.horsefield@biochemistry.lu.se.

This article contains supporting information online at www.pnas.org/lookup/suppl/doi:10.1073/pnas.1321406111/-/DCSupplemental.

tetramer and stabilize a specific conformation of the cytoplasmic loop D that is necessary for this interaction to occur. Radioligand binding studies show that oocytes expressing AQP2 bind Ca^{2+}, supporting Ca^{2+} as the physiological ligand for these sites. Several interactions that lead to NDI when disrupted by mutation are also highlighted. Together, this structure provides insights into AQP2 mutations in NDI and opens new opportunities to study the structural mechanism behind membrane protein sorting, including ER recognition of misfolded proteins.

Results

Crystallization of AQP2. Human AQP2 expressed in insect cells (17) has previously yielded 2D crystals diffracting to 4.5 Å resolution (18). Extensive efforts to produce better diffracting 3D crystals using full-length human AQP2 produced in insect cells failed to sufficiently improve the diffraction. AQP2 was therefore C-terminally truncated at Pro242 and expressed in *Pichia pastoris*. Pro242 corresponds to the last visible residue in the structure of human AQP5 (19), AQP2's closest paralog with which it shares 63% sequence identity (19). With this truncated AQP2, significant improvement in diffraction quality was achieved. Complete data to 2.75 Å were collected on a single frozen crystal (Table 1), yielding a molecular replacement solution using a homology model based on human AQP5 (19). Iterative rounds of manual rebuilding and structural refinement resulted in a model with an *R*-factor and free *R*-factor of 20.2% and 22.5%, respectively (for typical electron density, see Fig. S2). Of particular significance, these crystals belonged to the space group $P4_2$ with one tetramer in the asymmetric unit, whereby structural differences between individual protomers within the tetramer can be observed.

Crystal Structure of AQP2. AQP2 displays the conserved aquaporin fold, assembling as a tetramer with each protomer consisting of six transmembrane helices. Two half-membrane spanning helices, formed by loops B and E, constitute a seventh pseudotransmembrane segment (Fig. 1 *A* and *B*). Each protomer contains a water-conducting pore through which water is transported in a single file. Two conserved regions are of particular interest within this pore: the NPA region, containing two copies of the Asn–Pro–Ala (NPA) aquaporin signature motif, and the aromatic/arginine selectivity filter (ar/R), which determines transport specificity (20) (Fig. S3).

Table 1. Crystallographic data and refinement statistics

Data collection	
Beamline/wavelength	ESRF ID14-4/0.939
Space group	$P4_2$
Cell dimensions, a, b, c, Å	119.11, 119.11, 90.62
Resolution, Å	119.1–2.75 (2.9–2.75)
No. of reflections	33,066 (4,805)
R_{merge}/R_{pim}	0.095 (1.055)/0.044 (0.630)
CC1/2	0.453
I/σI	9.2 (1.3)
Completeness/redundancy	99.9 (99.8)/4.2 (3.7)
Refinement	
Resolution, Å	50.0–2.75 (2.95–2.75)
R_{work}/R_{free}*	0.202/0.225 (0.224/0.247)
Average B-factors, $Å^2$	89.9
r.m.s.d. from restraint target values	
Bond lengths, Å/angles, °	0.009/1.13
Ramachandran plot analysis, %	
Favored/allowed/disallowed	87.4/12.6/0.0
PDB code	4NEF

Number in parentheses is for highest resolution shell.
*R_{free} was calculated for 5% of reflections randomly excluded from the refinement.

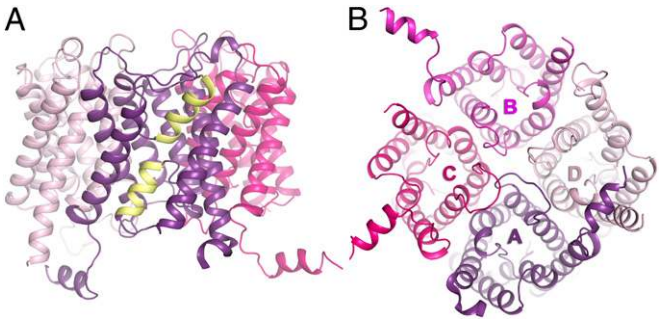

Fig. 1. Overall structure of human AQP2. (*A*) Overview of the AQP2 tetramer with half helices formed by loops B and E highlighted in yellow. (*B*) Overview of the AQP2 tetramer from the intracellular side. The color scheme for each of the protomers is used throughout the article (A, purple; B, magenta; C, pink; D, light pink).

When calculated using HOLE (21), all protomers show a similar pore profile, with the ar/R region constituting its narrowest point with an average diameter of 1.8 Å (Fig. S4).

C Termini Show Significant Conformational Variability. A striking difference between the X-ray structure of AQP2 and all other mammalian AQP structures is the highly variable position of the short C-terminal helix (Fig. 2*A*). This flexibility is likely to have hindered full-length AQP2 from yielding well-diffracting crystals. The C-terminal helix adopts a unique conformation in each of the four AQP2 protomers, and in one protomer (D), it is highly disordered. None of these conformations have previously been observed in mammalian AQP structures (19, 22–24), for all of which the C-terminal helix lies across the AQP cytoplasmic surface with only small variations between structures. In one protomer, the C-terminal helix interacts with a symmetry-related AQP2 molecule, forming one of several interactions that are important for crystal contacts. Specifically, four hydrophobic leucine residues (Leu230, 234, 247, and 240) that align on the same side of the C-terminal helix of protomer C are sheltered from exposure to the cytoplasm by this helix inserting into the cytoplasmic vestibule on the surface of protomer D of another AQP2 tetramer (Fig. 2*B*). This interaction is further stabilized by hydrogen bonds between side chains and main-chain carbonyls (Fig. S5).

An unusual flexibility in the AQP2 C terminus is likely to arise from two consecutive prolines (Pro225 and Pro226) that form a hinge region, whereas only one proline residue is present in the corresponding position in other mammalian AQP structures. In particular, the second proline may be functionally important in AQP2 trafficking, as the P226A mutant caused ER retention in Madin–Darby canine kidney cells, whereas the P225A mutant did not (25). However, whether this flexibility is important for phosphorylation and ubiquitination of the C terminus, events that are critical for AQP2 trafficking to and from the apical membrane, remains to be demonstrated.

***N* Termini Adopt Two Distinct Conformations.** For the AQP2 N terminus, two distinct conformations can be seen (Fig. 2*C*), although this region is disordered before residue six in protomers B and C. In protomer A, the N terminus adopts a conformation allowing hydrogen bond interactions to form between Glu3, Ser82, and Arg85. This structural triad is also observed in human AQP5 (19) and in the spinach water channel plasma membrane intrinsic protein 2;1 (SoPIP2;1) (26), where for the latter it is proposed to play an important role in the gating mechanism. In contrast, protomer D of AQP2 adopts a conformation similar to that seen in AQP1, with transmembrane (TM) helix 1 extending an additional full turn into the cytoplasm. This conformation was also observed in the phospho-mimicking S115E mutant of

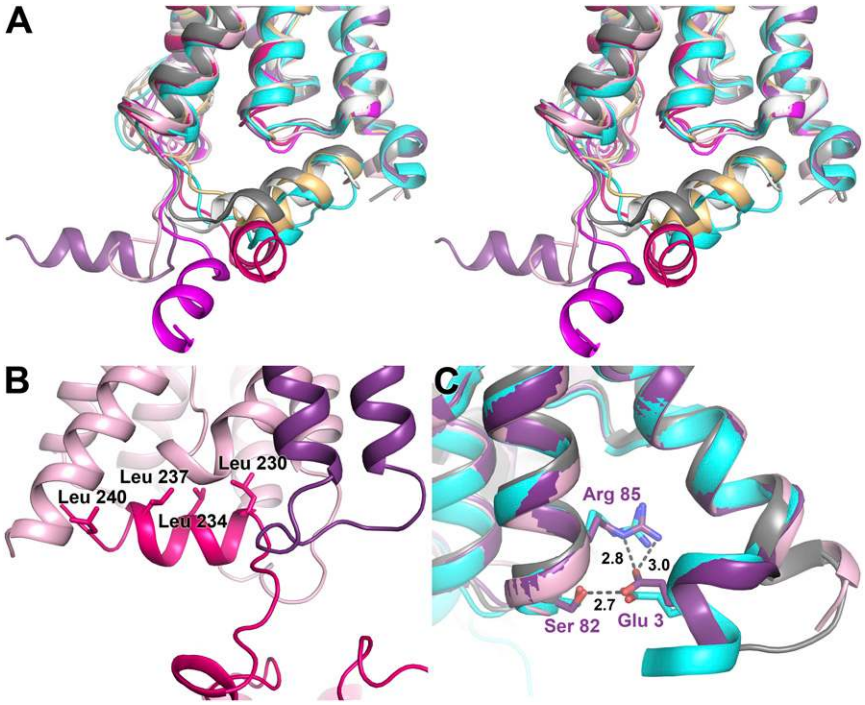

Fig. 2. Structure of the C and *N* termini. (*A*) Stereo image of the four AQP2 protomers (colored as in Fig. 1) overlaid on OaAQP0 [white; Protein Data Bank (PDB) ID code 2B60], BtAQP0 (light orange; PDB ID code 1YMG), BtAQP1 (gray; PDB ID code 1J4N), and HsAQP5 (cyan; PDB ID code 3D9S). The C termini of all four AQP2 protomers occupy different positions, none of which overlay with any of the previous AQP structures. (*B*) The crystal contact site between the C-terminal helix of monomer C (pink) and a symmetry-related protomer D (light pink). Leucines lining up on one side of the helix are labeled. (*C*) Overlay of the *N* termini of protomer A and D with HsAQP5 (cyan) and BtAQP1 (gray). For protomer A (purple), Glu3 interacts with Ser82 and Arg85, similar to the structural arrangement seen in AQP5. In contrast, protomer D (light pink) resembles BtAQP1 with TM helix 1 extending a full turn into the cytoplasm.

SoPIP2;1, where the extension of TM helix 1 disrupts a Ca^{2+} binding site implied in gating (27). The reoccurrence of these two specific N-terminal conformations among regulated eukaryotic aquaporins suggests a structural principle governing their regulation. Indeed, the AQP2 N terminus is important for trafficking, as exchanging both the *N* and C termini of AQP1 for those of AQP2 was needed to transpose 1-desamino-8-D-arginine vasopressin–regulated shuttling, a characteristic of AQP2, onto AQP1 (25).

AQP2 Binds Cd^{2+} at Two Sites. Two prominent peaks, visible at 14 σ and 8.7 σ, respectively (σ is the SD of the map), were found in the AQP2 F^{obs}–F^{calc} residual electron density map. Corresponding difference density peaks were also seen in the F^{obs}–F^{obs} anomalous difference density map (9.4 σ and 4.5 σ, respectively), specifically indicating the presence of a heavy metal. Because $CdCl_2$ was used as an additive during crystallization, these two peaks were assigned as Cd^{2+}, with two Cd^{2+} ions built per tetramer (Cd1 and Cd2) at the cytoplasmic side of the membrane (Fig. 3*A*). Cd1 has full occupancy, binds at the membrane interface between protomers A and D, and is ligated by GluA155 of loop D and GlnD57 of TM helix 2, as well as two water molecules (Fig. 3*B*). Cd2 has partial (65%) occupancy, is located between loop B and the C-terminal tail in protomer C, and is ligated by HisC80, GluC232, and one water molecule (Fig. 3*C*).

Cd^{2+} binding clearly influences the structure of loop D, which adopts different conformations in all four protomers (Fig. S6*A*). The binding of Cd1 displaces loop D of protomer A closer to the center of the AQP2 tetramer, where loop D of protomers A, B, and D all interact via hydrogen bonds between AsnA156, AsnD156, and GluB155 (Fig. S6*B*). In protomer D, this creates a binding pocket into which the C-terminal helix of a symmetry-related protomer C binds (Figs. 2*B* and 3*A*). Furthermore, the binding of Cd2 between loop B and the C terminus of protomer C helps position the C-terminal helix for this interaction (Fig. 3*A*). Thus, the binding of Cd^{2+} appears to be important for interactions between AQP2 tetramers within the crystal and explains why this additive was critical during crystal optimization.

Oocytes Expressing AQP2 Bind Ca^{2+}. Although Cd^{2+} binding is clearly important for crystal formation, this does not necessarily imply functional significance. A regulatory role for divalent cations was suggested from the crystal structure of the gated spinach aquaporin SoPIP2;1 in which binding of Cd^{2+} was observed to control the conformation of the gating element loop D (26). For SoPIP2;1 it was speculated that the Cd^{2+} ion is replaced by Ca^{2+} in vivo, and independent studies showed Ca^{2+} almost completely abolishing the water transport ability of PIP aquaporins (28).

To test whether AQP2 binds Ca^{2+}, we performed a radioactive calcium-binding assay. In this assay, either control or AQP2-expressing *Xenopus* oocytes were generated and their membranes isolated and incubated in medium containing $^{45}Ca^{2+}$. Following extensive washing, liquid scintillation counting revealed that significantly more $^{45}Ca^{2+}$ was bound to membranes of AQP2-expressing oocytes than to those of water-injected controls (Fig. 3*D*). These data strongly suggest that AQP2 binds Ca^{2+} and, as for SoPIP2;1, imply that the observed Cd^{2+} binding sites in the AQP2 structure represent Ca^{2+} binding sites in vivo.

Discussion

NDI-Causing Mutations in AQP2. NDI is characterized by the inability to concentrate urine and can lead to severe dehydration unless water intake is increased. Fifty-one different mutations in the AQP2 gene have been identified in patients suffering from NDI (15, 16), most of which lead to autosomal recessive NDI whereby AQP2 is misfolded, retained in the ER, and rapidly degraded. In some cases, however, ER-retained mutants have been shown to retain some functionality (29–32), indicating that the degree of misfolding can be minor.

The locations of thirty-one NDI-causing mutations are identified in the AQP2 crystal structure, most of which are located within the transmembrane region (Fig. 4*A*). These are typically situated at helix–helix interfaces and presumably disturb packing interactions and correct folding and/or assembly of the AQP2 tetramer (Fig. S7*A*). A number of other mutations are found within the water-conducting pore, affecting key functional residues such as Asn68, Ala70, and Pro185 of the NPA region or Arg187 of the selectivity filter, or causing pore narrowing as in

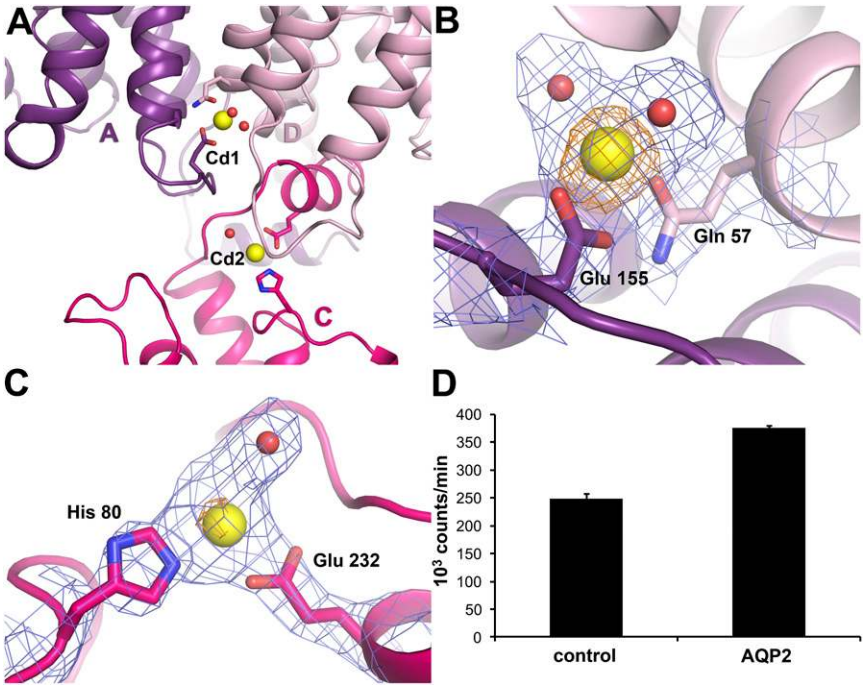

Fig. 3. Cd^{2+} binding sites in AQP2. (*A*) Two Cd^{2+} binding sites (Cd1 and Cd2) are found on the cytoplasmic side of the AQP2 tetramer. Yellow spheres represent Cd^{2+}. The interaction between the C-terminal helix of protomer C (pink) with protomer D (light pink) of a symmetry-related tetramer is also shown. (*B*) Electron density for the Cd1 site showing $2F^{obs}–F^{calc}$ map contoured at 1.5 σ (blue) and anomalous difference map contoured at 3.5 σ (orange). Residues serving as Cd^{2+} ligands are shown in stick representation. Water molecules ligating the Cd^{2+} ion are shown as red spheres. (*C*) Electron density for the Cd2 site showing a $2F^{obs}–F^{calc}$ map contoured at 1.2 σ (blue) and anomalous difference map contoured at 3.5 σ (orange). Cd^{2+} ligands are displayed as in *B*. (*D*) Radioactive Ca^{2+} binding assay illustrating how AQP2-expressing *Xenopus* oocytes bind significantly more $^{45}Ca^{2+}$ ($P < 0.05$) than controls, suggesting that Ca^{2+} is the physiological ligand for the Cd^{+} binding sites. Mean ± SEM is given of three groups of 10 oocytes per condition.

the case of V71M and V168M mutations (Fig. S7*B*). Precisely how these folding defects are recognized for retention in the ER and degradation cannot be deduced from the X-ray structure of only wild-type AQP2.

A small number of NDI-causing mutations are also found in loop regions. Within the extracellular loop C, mutation of Thr125 and Thr126 to methionine leads to autosomal recessive NDI (30, 31). These two threonines are situated close to an *N*-glycosylation site at Asn123. When compared against other mammalian AQPs that lack this glycosylation site, the structure of loop C is distinctly different for AQP2 (Fig. 4*B*). Glycosylation at this site has been suggested to be important for protein sorting in the Golgi complex, as AQP2–N123Q is retained in this organelle when expressed in renal cells (33). In oocytes, however, expression of AQP2–T125M and T126M leads to ER retention (31, 32), whereas the glycosylation mutant N123Q does not (33), suggesting that it might not be the lack of glycosylation per se that causes ER retention but rather mutation-induced structural changes within loop C.

Within the cytoplasmic loop D, the D150E mutant has been identified in patients suffering from recessive NDI (34, 35). Our X-ray structure reveals that Asp150 mediates an interaction between loop D and the proximal end of the C-terminal tail, with Asp150 connecting to Pro225 via hydrogen bonds mediated by Arg152 (Fig. 4*C*). This interaction is conserved in other mammalian AQP structures (19, 22–24, 36). For AQP5, it was argued that disturbing this interaction might cause structural changes to the C terminus that flags the protein for trafficking (19). It is certainly plausible that the bulkier glutamate head group of the AQP2 D150E mutant would perturb this network of hydrogen bonds, resulting in structural changes, which could be recognized by the ER quality control as misfolded protein.

Mutations Near Cd1 Cause ER Retention. Our crystal structure of AQP2 revealed two unanticipated Cd^{2+} binding sites per tetramer (Fig. 3*A*). It is therefore striking that mutation of the Cd1 ligand Gln57 to proline, which disrupts this divalent cation binding site, has been identified in NDI patients and shown to cause ER retention in oocytes (37). It is plausible that the loss of a divalent cation at this site flags AQP2 for ER retention. Mutation of Ser148, which is situated in a caseine kinase II consensus site at the cytoplasmic end of TM helix 4, also results in ER retention (6). The structure reveals that Ser148 of protomer A interacts with the Cd^{2+} ligand Gln57 through a direct hydrogen bond (Fig. 4*D*). This structural arrangement is strongly reminiscent of the gated spinach aquaporin SoPIP2;1, for which an interaction between Ser115 and the Cd^{2+} ligand Glu31 plays an important functional role by regulating the opening or closure of the channel (Fig. S8) (26). In SoPIP2;1, phosphorylation of Ser115 disrupts this interaction and perturbs the Cd^{2+} binding site, thereby inducing channel opening through a conformational change of cytoplasmic loop D (26, 27). Should Ser148 of AQP2 be phosphorylated, this could be signaled through a change in protein structure triggered by disruption of this divalent cation binding site.

An effect of putative phosphorylation of Ser148 of AQP2 was studied in oocytes by mutating this serine to alanine or aspartate to abolish or mimic phosphorylation, respectively (6). In these studies it was observed that the S148A mutant was properly targeted to the plasma membrane, whereas the S148D mutant was retained in the ER. Although no evidence for in vivo phosphorylation of Ser148 has been presented, it is intriguing that this serine-to-aspartate mutation, which almost certainly disrupts its interaction with the Cd^{2+} ligand Gln57, has such a clear effect on AQP2 trafficking, whereas replacement with alanine, which should not affect Cd^{2+} binding, does not. Moreover, an A147T mutation, the site adjacent to Ser148, has been identified in patients with autosomal recessive NDI, again due to ER retention of AQP2 (30). Although Ala147 does not directly interact with any Cd^{2+} ligand, mutation of this residue might perturb the Cd^{2+} binding site. Irrespective of its physiological significance, it is highly suggestive that missense mutation of three residues in close proximity to this divalent cation binding site causes ER retention. This indicates that this region is unusually sensitive to perturbations that result in the protein being viewed as misfolded by the ER quality control.

Potential Role for Ca^{2+} Binding in AQP2 Trafficking. Although Cd^{2+} is observed in the AQP2 structure because of its presence in the crystallization conditions, Ca^{2+} is a more likely physiological ligand. This argument is supported by our results from radioactive

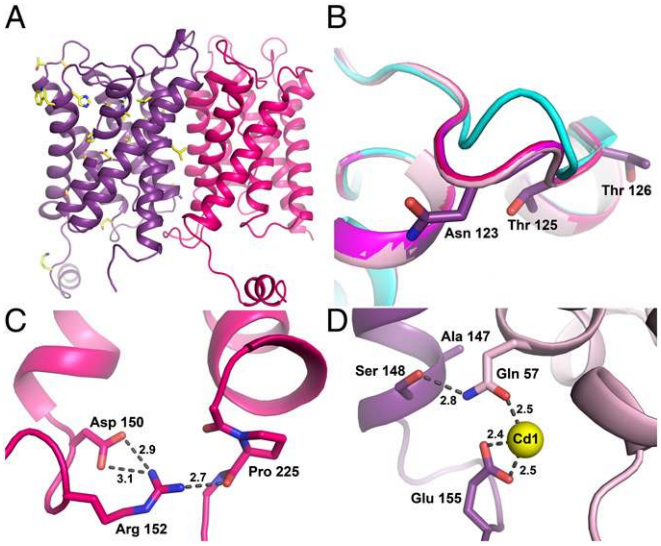

Fig. 4. NDI-causing mutations in AQP2. (*A*) Overview of known NDI-causing mutations (yellow) in the AQP2 structure showing how these mostly affect the pore-forming regions. (*B*) Structural overlay of loop C from the four AQP2s showing the *N*-glycosylation site at Asn123. A comparison with other mammalian AQPs, here represented by AQP5 (cyan), shows that structure of AQP2 is markedly different at this site. Asn123 as well as two nearby NDI mutation sites, Thr125 and Thr126, are shown in stick representation. (*C*) Structure around the NDI mutation site at Asp150, showing its connections to Pro225 at the proximal end of the C-terminal tail via Arg152. Hydrogen bonds are indicated by dotted lines. Distances are shown in Å. (*D*) Close-up of the Cd1 site showing how Ser148 hydrogen bonds to the Cd^{2+} ligand Gln57. Mutation of both these residues cause ER retention of AQP2. Bonds are indicated by dotted lines with distances shown in Å.

binding assays demonstrating that oocytes expressing AQP2 bind significantly more Ca^{2+} than control oocytes (Fig. 3*D*). Binding of AVP to the V2R triggers, besides a rise in cAMP level, an increase in intracellular Ca^{2+} levels (38–42). Moreover, AVP-induced plasma membrane sorting of AQP2 is reduced by calmodulin and ryanodine receptor inhibitors, indicating that release of intracellular Ca^{2+} from ryanodine-sensitive stores is important for AQP2 targeting to the apical membrane (43, 44). Because the AQP2 Ca^{2+} binding sites identified in the crystal structure are accessible from the cytoplasm, we hypothesize that transient changes in the intracellular Ca^{2+} concentration triggers changes in the structure of AQP2 and that these changes correlate with Ca^{2+}-dependent targeting of AQP2 to the apical membrane.

LIP5 Interacts with the C-Terminal Helix of AQP2. The presence of AQP2 in the apical membrane is affected not only by AVP-stimulated fusion of storage vesicles but also by the internalization rate upon cessation of the AVP signal. AQP2 internalization involves ubiquitination of Lys270 at the C terminus, which enhances endocytosis and targets AQP2 to multivesicular bodies (MVBs) for subsequent lysosomal degradation (10). A protein involved in MVB formation is the lysosomal trafficking regulator interacting protein 5 (LIP5). LIP5 is abundantly expressed in the collecting duct (45) and has been shown to interact with AQP2 and facilitate its lysosomal degradation (46).

Biochemical studies have localized the LIP5 binding site of AQP2 to residues 230–243, all of which are located within the AQP2 C-terminal helix (46). Moreover, LIP5 is known to bind proteins containing leucine-rich regions (47), and leucines 230, 234, 237, and 240 all align on the same side of the C-terminal helix in AQP2 (Fig. 2*B*). It is therefore intriguing that, for protomer C, this leucine-rich region interacts with the cytoplasmic surface of a symmetry-related AQP tetramer. We conclude that the observed interaction arises from the propensity of the C-terminal helix to participate in protein–protein interactions and similar interactions are presumably important in LIP5-mediated trafficking of AQP2.

An involvement of this short C-terminal helix in protein–protein interactions has also been reported for the AQP0–Calmodulin interaction in which one Calmodulin molecule binds the C-terminal helix from two AQP0 protomers simultaneously (48, 49). This interaction, which results in reduced AQP0 water permeability, was shown to be dependent on four hydrophobic residues (Leu227, Val230, Leu234, and Leu237) aligning on the same side of the C-terminal helix, as is observed for Leu230, Leu234, Leu237, and Leu240 in AQP2 (49). Furthermore, these authors state that rotational movements of the C-terminal helices are necessary for the interaction to occur. Hence, exposed hydrophobic residues on the aquaporin C-terminal helix may well be a reoccurring motif involved in AQP–protein interactions.

In the case of AQP2, several proteins have been suggested to interact with the AQP2 C terminus (50–52). Whether or not these interactions involve hydrophobic interfaces within the C-terminal helix remains to be shown. Nevertheless, we suggest that the conformational variability of the AQP2 C terminus seen in the crystal structure allows for exposure of a variety of binding surfaces, whereby interaction with a wide range of proteins can occur.

Conclusion

A major challenge in membrane protein structural biology is to take the step from understanding the structure–function relationships of individual membrane proteins to understanding how these are regulated by posttranslational modification and protein–protein interactions. AQP2 is the most clinically studied member of the aquaporin family and is by far the best characterized in terms of biosynthesis, trafficking from storage vesicles to the apical membrane and vice versa, degradation, posttranslational modifications, protein–protein interactions, as well as mutations in patients suffering from NDI. The crystal structure of AQP2 provides structural insights into all of these phenomena. A deeper understanding of how AQP2 mutants are recognized and retained in the ER, or how other proteins such as LIP5 interact with the C-terminal helix, will require further structural studies of AQP2 including complex structures with bound interaction partners. Our structure of AQP2, recovered through rational modification of the AQP2 construct, both deepens our understanding of its function in the human kidney and lays a platform from which protein–protein interactions regulating a membrane protein channel activity by trafficking can be explored.

Materials and Methods

Cloning, Overproduction, and Membrane Preparation. C-terminally truncated human AQP2 was cloned and transformed into *P. pastoris*. Cells were grown in a 3 L fermentor typically resulting in 500 g wt cells/L culture after 24 h of MeOH induction. After harvesting using centrifugation, cells were broken using a French Press and membranes were pelleted. The resulting membranes were washed in a urea buffer and stored at -80 °C until further use. For further details, see *SI Materials and Methods*.

Solubilization, Purification, and Crystallization. Membranes containing AQP2 was solubilized in 2% (wt/vol) n-nonyl-β-D-glucopyranoside (NG) by stirring for 1 h in an ice bath. AQP2 was purified and concentrated to a final concentration of 7.5 mg/mL (*SI Materials and Methods*). During the last purification step, the detergent was changed from NG to octylglucose–neopentylglycol (OGNPG). Crystals were obtained using the hanging drop vapor diffusion technique by mixing protein and reservoir [20–30% (vol/vol) PEG400, 0.1 M Tris pH 8, 0.1 M NaCl, 0.15 M $MgCl_2$] in a 1:1 ratio, with 0.1 M $CdCl_2$ added to the drop only (*SI Materials and Methods*). Rod-shaped crystals appeared within a few days. Following cryoprotection (*SI Materials and Methods*), crystals were flash frozen in liquid nitrogen and stored for data collection.

Data Collection and Structural Determination. Complete data at 100 K from a frozen crystal were collected at European Synchrotron Radiation Facility (ESRF), Grenoble, France. Crystals belonged to space group $P4_2$ with one tetramer in the asymmetric unit (a = 119.11 Å, b = 119.11 Å, c = 90.48 Å, $\alpha = \beta = \gamma = 90°$). Following processing and scaling of image data, the structure was solved by molecular replacement (*SI Materials and Methods*). Iterative rounds of refinement and manual model building (*SI Materials and Methods*) resulted in a model consisting of four protein chains (A–D) with the following residues—A2–240, B6–238, C6–241, and D2–233—two Cd^{2+} ions, one Zn^{2+} ion, and 59 water molecules. The final *R*-factor and free *R*-factor for this model is 20.2% and 22.5%, respectively.

Radioactive Calcium Binding Assay on Total Membranes of Oocytes. Oocytes were isolated and injected with 10 ng AQP2 cRNA in 50 nL water per oocyte or water and cultured for 3 d, after which membranes were prepared, incubated with $^{45}Ca^{2+}$, and washed (*SI Materials and Methods*). Following transfer to counting tubes, 4 mL of scintillation liquid was added and counted in Tri-Carb 299 TR liquid scintillation counter. High water permeability confirmed expression of AQP2. Each value consists of three independent groups of 10 oocytes each. The experiments were performed trice. The difference between groups was tested by Student *t* test. A P value < 0.05 was considered statistically significant.

ACKNOWLEDGMENTS. We are grateful to Gerhard Fischer for help with data collection. We also thank Monika Bollok, Rosemarie Friemann, Anna Backmark, and Jenny van Oostrum for contributions to the project. This work was supported by grants from Vetenskapsrådet (VR) (2010-5208, 2012-2849), Stiftelsen Olle Engkvist Byggmästare, European Membrane Protein Consortium (E-MeP) (LSHG-CT-2004-504601), and European Drug Initiative on Channels and Transporters (EDICT) (HEALTH-F4-2007-201924). P.M.T.D. is the recipient of VICI Grant 865.07.002 from the Netherlands Organization for Scientific Research.

1. Verbalis JG (2003) Disorders of body water homeostasis. *Best Pract Res Clin Endocrinol Metab* 17(4):471–503.
2. van Os CH, Deen PM, Dempster JA (1994) Aquaporins: Water selective channels in biological membranes. Molecular structure and tissue distribution. *Biochim Biophys Acta* 1197(3):291–309.
3. Noda Y, Sohara E, Ohta E, Sasaki S (2010) Aquaporins in kidney pathophysiology. *Nat Rev Nephrol* 6(3):168–178.
4. Fushimi K, Sasaki S, Marumo F (1997) Phosphorylation of serine 256 is required for cAMP-dependent regulatory exocytosis of the aquaporin-2 water channel. *J Biol Chem* 272(23):14800–14804.
5. Katsura T, Gustafson CE, Ausiello DA, Brown D (1997) Protein kinase A phosphorylation is involved in regulated exocytosis of aquaporin-2 in transfected LLC-PK1 cells. *Am J Physiol* 272(6 Pt 2):F817–F822.
6. van Balkom BW, et al. (2002) The role of putative phosphorylation sites in the targeting and shuttling of the aquaporin-2 water channel. *J Biol Chem* 277(44): 41473–41479.
7. Fenton RA, et al. (2008) Acute regulation of aquaporin-2 phosphorylation at Ser-264 by vasopressin. *Proc Natl Acad Sci USA* 105(8):3134–3139.
8. Xie L, et al. (2010) Quantitative analysis of aquaporin-2 phosphorylation. *Am J Physiol Renal Physiol* 298(4):F1018–F1023.
9. Hoffert JD, et al. (2008) Vasopressin-stimulated increase in phosphorylation at Ser269 potentiates plasma membrane retention of aquaporin-2. *J Biol Chem* 283(36): 24617–24627.
10. Kamsteeg EJ, et al. (2006) Short-chain ubiquitination mediates the regulated endocytosis of the aquaporin-2 water channel. *Proc Natl Acad Sci USA* 103(48):18344–18349.
11. Katsura T, et al. (1995) Constitutive and regulated membrane expression of aquaporin 1 and aquaporin 2 water channels in stably transfected LLC-PK1 epithelial cells. *Proc Natl Acad Sci USA* 92(16):7212–7216.
12. Nielsen S, et al. (1995) Vasopressin increases water permeability of kidney collecting duct by inducing translocation of aquaporin-CD water channels to plasma membrane. *Proc Natl Acad Sci USA* 92(4):1013–1017.
13. Schrier RW, Fassett RG, Ohara M, Martin PY (1998) Vasopressin release, water channels, and vasopressin antagonism in cardiac failure, cirrhosis, and pregnancy. *Proc Assoc Am Physicians* 110(5):407–411.
14. Deen PM, et al. (1994) Requirement of human renal water channel aquaporin-2 for vasopressin-dependent concentration of urine. *Science* 264(5155):92–95.
15. Moeller HB, Rittig S, Fenton RA (2013) Nephrogenic diabetes insipidus: Essential insights into the molecular background and potential therapies for treatment. *Endocr Rev* 34(2):278–301.
16. Wesche D, Deen PM, Knoers NV (2012) Congenital nephrogenic diabetes insipidus: The current state of affairs. *Pediatr Nephrol* 27(12):2183–2204.
17. Werten PJ, et al. (2001) Large-scale purification of functional recombinant human aquaporin-2. *FEBS Lett* 504(3):200–205.
18. Schenk AD, et al. (2005) The 4.5 A structure of human AQP2. *J Mol Biol* 350(2): 278–289.
19. Horsefield R, et al. (2008) High-resolution x-ray structure of human aquaporin 5. *Proc Natl Acad Sci USA* 105(36):13327–13332.
20. Tajkhorshid E, et al. (2002) Control of the selectivity of the aquaporin water channel family by global orientational tuning. *Science* 296(5567):525–530.
21. Smart OS, Goodfellow JM, Wallace BA (1993) The pore dimensions of gramicidin A. *Biophys J* 65(6):2455–2460.
22. Sui H, Han BG, Lee JK, Walian P, Jap BK (2001) Structural basis of water-specific transport through the AQP1 water channel. *Nature* 414(6866):872–878.
23. Gonen T, et al. (2005) Lipid-protein interactions in double-layered two-dimensional AQP0 crystals. *Nature* 438(7068):633–638.
24. Harries WE, Akhavan D, Miercke LJ, Khademi S, Stroud RM (2004) The channel architecture of aquaporin 0 at a 2.2-A resolution. *Proc Natl Acad Sci USA* 101(39): 14045–14050.
25. van Balkom BW, et al. (2004) Role of cytoplasmic termini in sorting and shuttling of the aquaporin-2 water channel. *Am J Physiol Cell Physiol* 286(2):C372–C379.
26. Törnroth-Horsefield S, et al. (2006) Structural mechanism of plant aquaporin gating. *Nature* 439(7077):688–694.
27. Nyblom M, et al. (2009) Structural and functional analysis of SoPIP2;1 mutants adds insight into plant aquaporin gating. *J Mol Biol* 387(3):653–668.
28. Maurel C (2007) Plant aquaporins: Novel functions and regulation properties. *FEBS Lett* 581(12):2227–2236.
29. Canfield MC, Tamarappoo BK, Moses AM, Verkman AS, Holtzman EJ (1997) Identification and characterization of aquaporin-2 water channel mutations causing nephrogenic diabetes insipidus with partial vasopressin response. *Hum Mol Genet* 6(11): 1865–1871.
30. Mulders SM, et al. (1997) New mutations in the AQP2 gene in nephrogenic diabetes insipidus resulting in functional but misrouted water channels. *J Am Soc Nephrol* 8(2): 242–248.
31. Marr N, et al. (2002) Cell-biologic and functional analyses of five new Aquaporin-2 missense mutations that cause recessive nephrogenic diabetes insipidus. *J Am Soc Nephrol* 13(9):2267–2277.
32. Marr N, Kamsteeg EJ, van Raak M, van Os CH, Deen PM (2001) Functionality of aquaporin-2 missense mutants in recessive nephrogenic diabetes insipidus. *Pflugers Arch* 442(1):73–77.
33. Hendriks G, et al. (2004) Glycosylation is important for cell surface expression of the water channel aquaporin-2 but is not essential for tetramerization in the endoplasmic reticulum. *J Biol Chem* 279(4):2975–2983.
34. Guyon C, et al. (2009) Characterization of D150E and G196D aquaporin-2 mutations responsible for nephrogenic diabetes insipidus: Importance of a mild phenotype. *Am J Physiol Renal Physiol* 297(2):F489–F498.
35. Iolascon A, et al. (2007) Characterization of two novel missense mutations in the AQP2 gene causing nephrogenic diabetes insipidus. *Nephron, Physiol* 105(3):33–41.
36. Ho JD, et al. (2009) Crystal structure of human aquaporin 4 at 1.8 A and its mechanism of conductance. *Proc Natl Acad Sci USA* 106(18):7437–7442.
37. Lin SH, et al. (2002) Two novel aquaporin-2 mutations responsible for congenital nephrogenic diabetes insipidus in Chinese families. *J Clin Endocrinol Metab* 87(6): 2694–2700.
38. Champigneulle A, Siga E, Vassent G, Imbert-Teboul M (1993) V2-like vasopressin receptor mobilizes intracellular Ca2+ in rat medullary collecting tubules. *Am J Physiol* 265(1 Pt 2):F35–F45.
39. Ecelbarger CA, Chou CL, Lolait SJ, Knepper MA, DiGiovanni SR (1996) Evidence for dual signaling pathways for V2 vasopressin receptor in rat inner medullary collecting duct. *Am J Physiol* 270(4 Pt 2):F623–F633.
40. Maeda Y, Han JS, Gibson CC, Knepper MA (1993) Vasopressin and oxytocin receptors coupled to Ca2+ mobilization in rat inner medullary collecting duct. *Am J Physiol* 265(1 Pt 2):F15–F25.
41. Star RA, Nonoguchi H, Balaban R, Knepper MA (1988) Calcium and cyclic adenosine monophosphate as second messengers for vasopressin in the rat inner medullary collecting duct. *J Clin Invest* 81(6):1879–1888.
42. Yip KP (2002) Coupling of vasopressin-induced intracellular Ca2+ mobilization and apical exocytosis in perfused rat kidney collecting duct. *J Physiol* 538(Pt 3):891–899.
43. Levine SD, Kachadorian WA, Levin DN, Schlondorff D (1981) Effects of trifluoperazine on function and structure of toad urinary bladder. Role of calmodulin vasopressin-stimulation of water permeability. *J Clin Invest* 67(3):662–672.
44. Chou CL, et al. (2000) Regulation of aquaporin-2 trafficking by vasopressin in the renal collecting duct. Roles of ryanodine-sensitive Ca2+ stores and calmodulin. *J Biol Chem* 275(47):36839–36846.
45. Boone M, et al. (2010) The lysosomal trafficking regulator interacting protein-5 localizes mainly in epithelial cells. *J Mol Histol* 41(1):61–74.
46. van Balkom BW, et al. (2009) LIP5 interacts with aquaporin 2 and facilitates its lysosomal degradation. *J Am Soc Nephrol* 20(5):990–1001.
47. Skalicky JJ, et al. (2012) Interactions of the human LIP5 regulatory protein with endosomal sorting complexes required for transport. *J Biol Chem* 287(52):43910–43926.
48. Reichow SL, Gonen T (2008) Noncanonical binding of calmodulin to aquaporin-0: Implications for channel regulation. *Structure* 16(9):1389–1398.
49. Reichow SL, et al. (2013) Allosteric mechanism of water-channel gating by Ca2+-calmodulin. *Nat Struct Mol Biol* 20(9):1085–1092.
50. Noda Y, et al. (2004) Aquaporin-2 trafficking is regulated by PDZ-domain containing protein SPA-1. *FEBS Lett* 568(1-3):139–145.
51. Lu HA, et al. (2007) Heat shock protein 70 interacts with aquaporin-2 and regulates its trafficking. *J Biol Chem* 282(39):28721–28732.
52. Kamsteeg EJ, et al. (2007) MAL decreases the internalization of the aquaporin-2 water channel. *Proc Natl Acad Sci USA* 104(42):16696–16701.